

## Article

# A Study of the Field of View Performance for Full-Color Waveguide Displays Based on Polarization Volume Gratings

Yuchen Gu , Yishi Weng <sup>\*</sup>, Yuning Zhang, Chuang Wang, Ran Wei, Wei Wang, Nan Lin, Lixuan Zhang and Baoping Wang

Joint International Research Laboratory of Information Display and Visualization, School of Electronic Science and Engineering, Southeast University, Nanjing 210018, China

\* Correspondence: yishi@seu.edu.cn

**Abstract:** Multilayer waveguide structures can realize full-color AR displays of diffractive waveguides. This paper discusses the field-of-view characteristics of a waveguide system with a multilayer structure when polarization volume gratings (PVG) are applied as couplers to achieve a full-color display. The effects of the refractive index and period parameter of PVG-couplers on the field of view are investigated. In addition, a PVG waveguide sample with an optimized design is prepared. The experimental results show that the designed waveguide system can achieve a full-color AR display with a 45° diagonal field of view, which verifies the feasibility of the design and provides a potential solution for AR color waveguide display applications.

**Keywords:** polarization volume grating; field of view; waveguide display; full-color



**Citation:** Gu, Y.; Weng, Y.; Zhang, Y.; Wang, C.; Wei, R.; Wang, W.; Lin, N.; Zhang, L.; Wang, B. A Study of the Field of View Performance for Full-Color Waveguide Displays Based on Polarization Volume Gratings. *Crystals* **2022**, *12*, 1805. <https://doi.org/10.3390/cryst12121805>

Academic Editor: Ingo Dierking

Received: 30 November 2022

Accepted: 9 December 2022

Published: 12 December 2022

**Publisher's Note:** MDPI stays neutral with regard to jurisdictional claims in published maps and institutional affiliations.



**Copyright:** © 2022 by the authors. Licensee MDPI, Basel, Switzerland. This article is an open access article distributed under the terms and conditions of the Creative Commons Attribution (CC BY) license (<https://creativecommons.org/licenses/by/4.0/>).

## 1. Introduction

Flat panel displays currently suffer from the contradiction between information capacity, portability and power consumption, so people are actively exploring next-generation display technologies. AR near-eye display devices are considered the next generation of information display terminals due to their wearability, translucency, and ability to achieve huge screen displays with low power consumption. The wavelength and angular selectivity of the liquid crystal optical elements (LCOEs) allow the see-through view of the real scene to be transmitted to the eye unaltered, thereby enabling an optical see-through AR configuration. In the meantime, LCOEs can be made on very thin substrates, allowing the display system to have a favorable profile and be lightweight for a better wearing experience for the user.

Research on LCOEs with photoalignment techniques began in the early 1980s [1]. Since then, recording materials and methods have been steadily improved. Currently, Pancharatnam-Berry (PB) phase gratings [2,3] or lens [4–7], cholesteric liquid crystal (CLC) reflectors [8], and polarization volume gratings (PVG) [9–14] or lens (PVL) [15–17] are the main LCOEs used for near-eye displays. In the current near-eye display, waveguide display solutions are one of the industry's focuses. As PVG overcomes the problems of low efficiency of surface relief grating (SRG) and narrow response bandwidth of volume holographic grating (VHG), PVG-based waveguide displays have been widely studied and demonstrated in recent years. Weng et al. proposed a dual-layer PVG-based waveguide solution to achieve a full-color AR display with a 35° diagonal field of view (FOV) [18]. The dual-layer structure is specifically a blue composite green sharing one layer of the waveguide, with red propagating independently in another layer of the waveguide. Cui et al. demonstrated a PVG-based waveguide display system with a 35° diagonal FOV using an "L" shaped two-dimensional exit pupil expansion structure [19]. Then, Gu et al. superimposed PVGs with different polarization responses as coupling elements and extended the angular response bandwidth by stacking PVGs to improve the efficiency and

FOV of the waveguide system [20]. However, the limits of the FOV that can be achieved with PVG-based waveguide displays have not been explored, especially in the case of full-color waveguide displays.

To enable a better understanding of the design challenges of PVG-based waveguides, this paper presents different schemes for realizing full-color diffractive waveguide display, including single-layer waveguides, dual-layer waveguides, and three-layer waveguides, providing an analysis of the FOV that such schemes can support. And in combination with bandwidth compounding [20], we simulate and experimentally demonstrate a dual-layer PVG-based waveguide RGB display scheme that achieves the same RGB FOV as the three-layer waveguide while reducing the size of the three-layer waveguide.

## 2. Device Design and Simulation

PVG has a complex three-dimensional helical structure, which tends to have the lowest free energy state [21]. As sketched in Figure 1a, the azo molecular compound at the bottom acts as an optical orientation layer, which shows a sinusoidal pattern along the  $x$ -axis. Meanwhile, there exists a transition region in which the liquid crystal molecules change from planar to three-dimensional helical orientation [22], and there exists a grating inclination angle  $\varphi$ , which satisfies the Bragg equation:

$$\begin{aligned} n_{eff} * p * \cos(\varphi + \theta_B) &= \lambda_B, \\ p &= 2\Lambda_b = 2\Lambda_x \sin \varphi \end{aligned} \quad (1)$$

where  $n_{eff}$  is the average refractive index of the PVG material,  $p$  is the length of the liquid crystal molecule rotated by  $360^\circ$ ,  $\theta_B$  is the Bragg angle,  $\lambda_B$  is the PVG Bragg wavelength,  $\Lambda_b$  is the PVG Bragg period and  $\Lambda_x$  is the PVG lateral period. The self-assembled helical structure has sensitive polarization response characteristics. For the PVG with a left-handed helical structure, when the incident light is left-handed circularly polarized (LCP), strong primary diffraction will occur, while when the incident light is right-handed circularly polarized (RCP), the light will pass directly through the grating without diffraction.

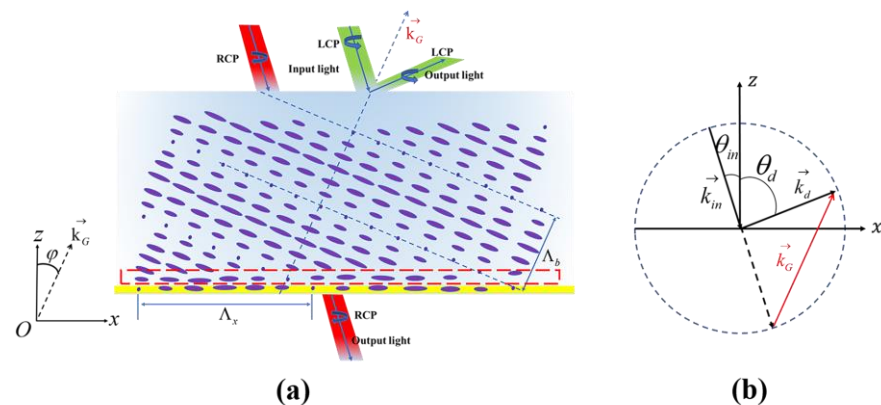


**Figure 1.** (a) Diagrams of the tilted helical structure of PVG. (b) Sketch of the relation among input, output, and grating vectors to satisfy the Bragg condition.

To satisfy the Bragg condition, Figure 1b shows that the  $k$ -vector of the incident light, diffracted light and the grating vector should form a triangular relationship:  $\vec{k}_{in} + \vec{k}_G = \vec{k}_d$ . When the incident light is coupled into the PVG waveguide from air, and the total internal reflection (TIR) occurs, the diffraction angle  $\theta_d$  (in waveguide media with refractive index  $n_{glass}$ ) and the incident angle  $\theta_{in}$  (in air) should satisfy:

$$\frac{2\pi}{\lambda} \sin \theta_{in} + \frac{2\pi}{\Lambda_x} = n_{glass} \frac{2\pi}{\lambda} \sin \theta_d, \quad (2)$$

where  $\lambda$  is the wavelength of the incident light in a vacuum. The diffraction angle is limited by the refractive index of the waveguide and must be greater than the TIR:

$$\theta_{d \min} = \arcsin \frac{1}{n_{glass}}, \quad (3)$$

The corresponding incident angle is

$$\sin \theta_{Rin} = 1 - \frac{\lambda}{\Lambda_x}, \quad (4)$$

Equation (4) shows that one boundary of the FOV is not affected by the refractive index of the waveguide but is closely related to the ratio of the incident wavelength to the PVG lateral period. Assuming that the maximum propagation angle in the waveguide is  $\theta_{dmax}$ , the corresponding incident angle is

$$\sin \theta_{Lin} = n_{glass} \sin \theta_{dmax} - \frac{\lambda}{\Lambda_x}, \quad (5)$$

Therefore, the FOV can be calculated as

$$\text{FOV} = \arcsin(n_{glass} \sin \theta_{dmax} - \frac{\lambda}{\Lambda_x}) - \arcsin(1 - \frac{\lambda}{\Lambda_x}). \quad (6)$$

It is important to note that the FOV mentioned here refers to the horizontal FOV in air, as well as the FOV not specifically described below. From the above equation, it seems that the FOV is related to  $n_{glass}$ , and the FOV increases as  $n_{glass}$  increases. However, for VHG or PVG, the incident light is diffracted inside the grating, so the diffraction angle inside the grating cannot exceed 90 degrees:

$$\theta_{dmax} < \theta'_{dmax} = \arcsin \frac{n_{eff}}{n_{glass}}. \quad (7)$$

This requires a matching refractive index between the grating and the waveguide medium. Otherwise, the upper limit of the propagation angle will be greatly limited. When the refractive index of the waveguide medium is matched with the refractive index of the grating material,  $\theta_{dmax}$  is determined by the allowable collimator aperture  $W$  and the thickness of the waveguide  $t$ :

$$\theta_{dmax} < \theta''_{dmax} = \arctan(\frac{W}{2t}). \quad (8)$$

FOV can be described as:

$$\text{FOV} = \begin{cases} \arcsin(1 - \frac{\lambda}{\Lambda_x}) - \arcsin(n_{eff} - \frac{\lambda}{\Lambda_x}) & n_{eff} < n_{glass}, \theta'_{dmax} < \theta''_{dmax} \\ \arcsin(n_{glass} \sin(\arctan(\frac{W}{2t})) - \frac{\lambda}{\Lambda_x}) - \arcsin(1 - \frac{\lambda}{\Lambda_x}) & \theta'_{dmax} > \theta''_{dmax} \end{cases}. \quad (9)$$

In the actual design application, we first choose the  $n_{glass}$  matching with  $n_{eff}$ . The  $W$  and  $t$  used in this paper are set to 18 mm and 0.7 mm, respectively, and the relationship between FOV and  $\frac{\lambda}{\Lambda_x}$ , in this case, is shown in Figure 2. The FOV is in an approximately symmetric trend with the  $\frac{\lambda}{\Lambda_x}$ . When  $\Lambda_x$  approaches 0.5 times or 1.78 times the value of  $\lambda$ , the FOV tends to the maximum. And since the larger the  $\Lambda_x$  is in the PVG preparation process, the better the arrangement of PVG liquid crystal molecules will be, so we prefer a larger  $\Lambda_x$  when designing a large FOV.

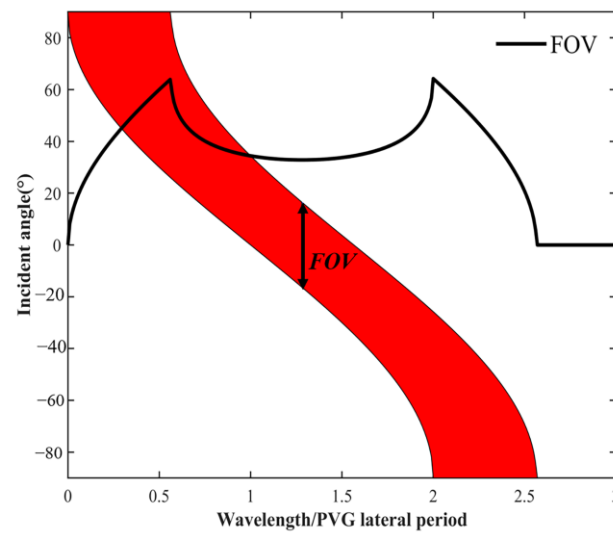


**Figure 2.** The curve of FOV and  $\frac{\lambda}{\Lambda_x}$  was plotted.

The simplest way to achieve a full-color waveguide display is to use stacked waveguides, each designed for a single color (R, G, or B), and by adjusting the diffraction angle of the grating, the maximum RGB FOV can be obtained. Independent three-layer waveguides are used to transmit R, G and B band beams, respectively. Since the beam propagation of the three bands is independent, the diffraction angles of the corresponding three coupled beams can be designed independently as needed without worrying about crosstalk. The architecture is currently used in many SRG waveguides, such as HoloLens 1 and Magic Leap One. When designing a PVG-based full-color waveguide, as shown in Figure 2, it is sufficient to obtain a corresponding  $\frac{\lambda}{\Lambda_x}$  according to the desired FOV, and thus the suitable  $\Lambda_x$  can be obtained for different wavelengths of incident light. The RGB FOV of the three-layer color waveguide structure is comparable to the monochromatic case. However, the main drawback of this structure is that it leads to an inevitable increase in the size and weight of the system.

PVG composite technology allows for a single-layer color waveguide system structure, thus minimizing the thickness and weight of the waveguide. A single-layer waveguide is a composite of red PVG, green PVG, and blue PVG in some form, and the coupled beam is transmitted within the same waveguide. This structure keeps the thickness and weight within the desired range because there is only a single layer of waveguide medium. Nevertheless, the single-layer waveguide structure has strict requirements for coupling composite gratings. Specifically, the R, G, and B grating components of the composite grating need to have an equal lateral period so that R, G and B grating components have the same dispersion curve, otherwise severe crosstalk will occur between the different grating components, leading to dispersion and ghosting in the final image. Figure 3a plots the curves for different values of  $\Lambda_x$  corresponding to different incident angle ranges at R (633 nm), G (519 nm), and B (448 nm) bands in the single-layer RGB waveguide structure. When  $\Lambda_x$  is very small, R and B cannot be transmitted in the waveguide at the same time (black dashed box), which confirms the wisdom of our previous choice of large  $\Lambda_x$ . In the case of large  $\Lambda_x$ , it is difficult to couple all RGB light into the waveguide over a large angular range if  $\Lambda_x$  is fixed for R, G, and B (Figure 3b). Compared to the three-layer waveguide solution, RGB FOV will obviously have a significant loss.

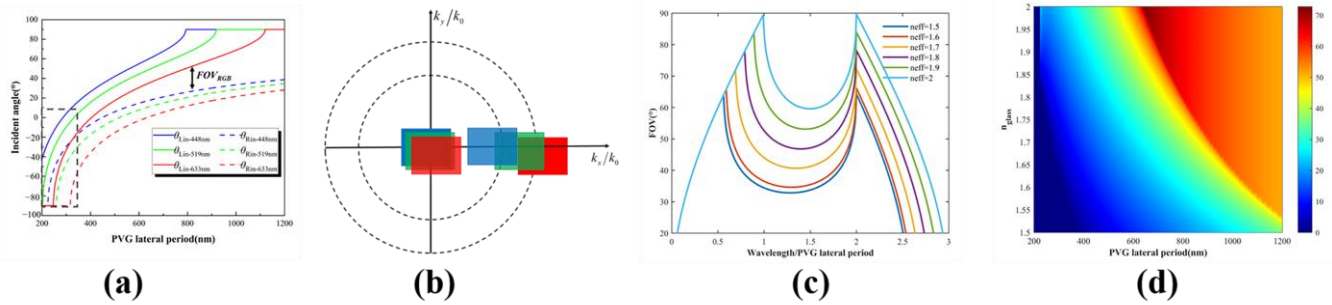


**Figure 3.** (a) Plot of the relationship between  $\Lambda_x$  and incident angle ranges at R (633 nm), G (519 nm), and B (448 nm) bands in the single-layer RGB waveguide structure. (b) k-vector diagram of the single-layer RGB waveguide. (c) Plot of the relationship between  $\frac{\lambda}{\Lambda_x}$  and FOV for different  $n_{eff}$  values. (d) Plot of the relationship between  $\Lambda_x$  and FOV with different  $n_{eff}$  values at R (633 nm), G (519 nm), and B (448 nm) bands in the single-layer RGB waveguide structure.

Since the  $n_{eff}$  of the PVG material we prepare is around 1.57,  $n_{glass}$  is also chosen to be 1.57, and the diffraction angle will be distributed in a limited range of waveguide propagation angles according to the dispersion curve, thus limiting FOV. If we want to achieve a larger FOV, we need to increase  $n_{eff}$  and the corresponding  $n_{glass}$ . As shown in Figure 3c, when the refractive index reaches 2, the FOV can reach about 90°. At the same time, the tilt angle between the light engine and the waveguide sheet can be smaller if a larger FOV is desired. Similarly, the RGB FOV of the single-layer waveguide becomes larger as  $n_{eff}$  and  $n_{glass}$  increase. As shown in Figure 3d, the RGB FOV of single-layer waveguides can also achieve up to nearly 70°. Relevant materials for high-refractive-index waveguide media are available, so it is necessary to find suitable high-refractive-index PVG materials in the future.

A dual-layer PVG RGB waveguide proposed by Weng et al. [18] reduces the weight and volume of the three-layer waveguide while also avoiding the small FOV of the single-layer waveguide [18]. Their scheme is to share one layer of waveguide for B and G and propagate R separately, as is shown in Figure 4a,b. When blue and green are in the same layer of the waveguide, and when we ensure that one of the color components propagates with full FOV, there inevitably exists a portion of the FOV of the other color component that cannot satisfy the propagation conditions of the waveguide. Figure 4c shows the incident angles satisfying the propagation conditions of G (519 nm) and B (448 nm) at different  $\Lambda_x$  values. In this instance, the FOV can be expressed as:

$$FOV_{BG} = \theta_{Lin-519nm} - \theta_{Rin-448nm} \tag{10}$$

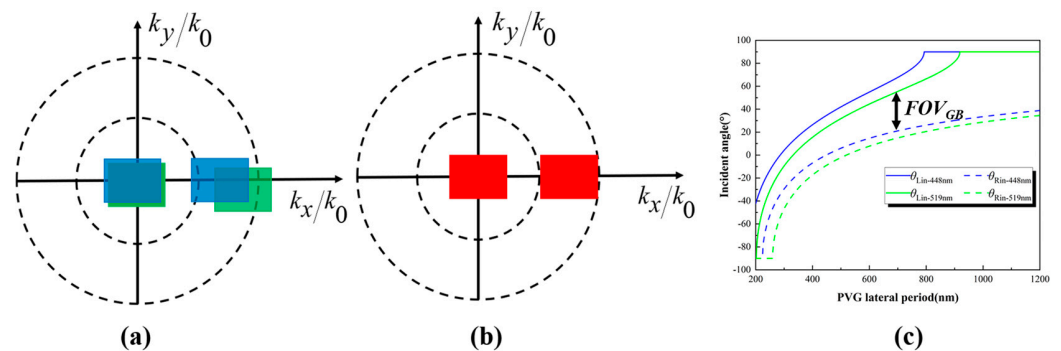


**Figure 4.** (a) The k-vector diagram for blue and green sharing a layer of the waveguide. (b) The k-vector diagram for red with a separate layer of the waveguide. (c) Plot of the relationship between  $\Lambda_x$  and incident angle ranges at the G (519 nm) and B (448 nm) bands in the common waveguide layer.

Another PVG-based dual-layer RGB waveguide is proposed in this paper, as shown in Figure 5a. This structure places B and G1 in the same waveguide and G2 and R in the same waveguide. As can be seen in Figure 5b, G1 is responsible for the green left part of the FOV and G2 is responsible for the green right FOV. G1 and G2 have partially overlapping FOVs in some cases (Figure 5c). To prevent the problem that the light diffracted by G1 is diffracted again by G2 during the propagation to the human eye in the out-coupling grating region, we can use G1 and G2 with different polarization responses in the out-coupling region. This dual-layer RGB waveguide can effectively reduce the size and weight of conventional three-layer RGB waveguides and maintain the same FOV as three-layer RGB waveguides.

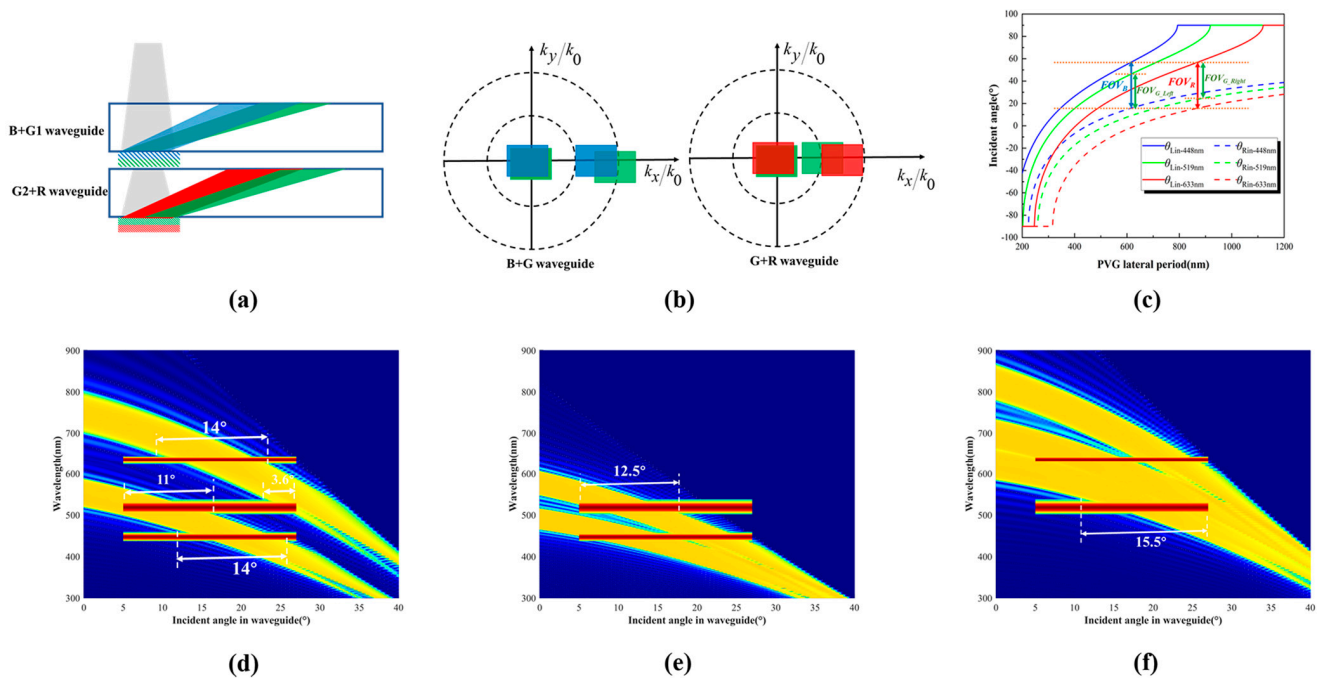


**Figure 5.** (a) Schematic diagram of the designed waveguide structure. (b) The k-vector diagram of the designed dual-layer RGB waveguide structure. (c) Plot of the relationship between  $\Lambda_x$  and incident angle ranges at the R (633 nm), G (519 nm), and B (448 nm) bands in the designed dual-layer RGB waveguide structure. (d) Wavelength-incidence-efficiency plot of Uncompounded PVGs. The red line is the light engine spectrum. (e) Wavelength-incidence-efficiency plot of compounded PVGs (corresponding to B+G1 waveguide). (f) Wavelength-incidence-efficiency plot of compounded PVGs (corresponding to R+G2 waveguide).

In order to match the light engine used in the experimental section, we need to select a suitable PVG lateral period. The diagonal field of view of the light engine used in the experimental section is  $45^\circ$  (resolution 4:3), so the lateral field of view needs to be guaranteed to be about  $36^\circ$ . According to Figure 2, we can calculate that the R (633 nm) PVG lateral period needs to be set near 705 nm, and the B (448 nm) PVG lateral period needs to be set near 501 nm. In the PVG preparation process, the lateral period is determined by the exposure angle and based on the current accuracy of our exposure rotary table of only  $1^\circ$ , the final R (633 nm) PVG lateral period is set to 739.44 nm, and the Bragg angle is  $16.62^\circ$ , and the B (448 nm) PVG lateral period is set to 521.25 nm, and the Bragg angle is  $16.62^\circ$ . The FOV of this light engine ranges from  $8.6^\circ$  to  $44.6^\circ$  (in air). For the efficiency of the PVGs in Figure 5d, the red band FOV supported is only  $14^\circ$  ( $22.3^\circ$  in air), and the blue band FOV supported is only  $14^\circ$  ( $22.3^\circ$  in air). And the FOV of the green band is divided into  $8.6^\circ$ – $26.5^\circ$  (in air) and  $39^\circ$ – $44.6^\circ$  (in air) under the circumstances.

We need to fill in the missing part of the FOV with laminated composite PVGs [20]. We superimposed three layers of PVG in the R+G2 waveguide and two layers of PVG in the B+G1 waveguide. The parameters for the design of each layer of PVG are shown

in Table 1. As shown in Figure 5e,f, the FOV of the red band of the light engine will be fully displayed in the R+G2 waveguide, the blue band will be fully displayed in the B+G1 waveguide, and the green band will be fully displayed in the B+G1 waveguide ( $8.6^{\circ}$ – $29^{\circ}$  in air) and R+G2 waveguide ( $17.5^{\circ}$ – $44.6^{\circ}$  in air), respectively. We also simulated the efficiency distribution of the horizontal FOV and vertical FOV for this design parameter (Figure 6). The horizontal coordinates represent the range of incident light angles along the waveguide propagation direction, and the vertical coordinates represent the range of incident light angles perpendicular to the waveguide propagation direction. We designed the incident light wavelengths as R (633 nm), G (519 nm), and B (448 nm), respectively. Red and blue propagate with an entire FOV in their respective waveguides, while the green FOV is split into two parts to propagate. Both horizontal and vertical field-of-view angles are satisfied with this structure.

**Table 1.** Design parameters of PVGs in the R+G2 waveguide and B+G1 waveguide.

	Bragg Wavelength (nm)	Bragg Angle ( $^{\circ}$ )	Bragg Period (nm)
R+G2 waveguide	633	18.199	230.9412
	633	22.293	280.5012
	633	16	203.8177
B+G1 waveguide	448	18.182	162.6483
	448	22.15	196.5275

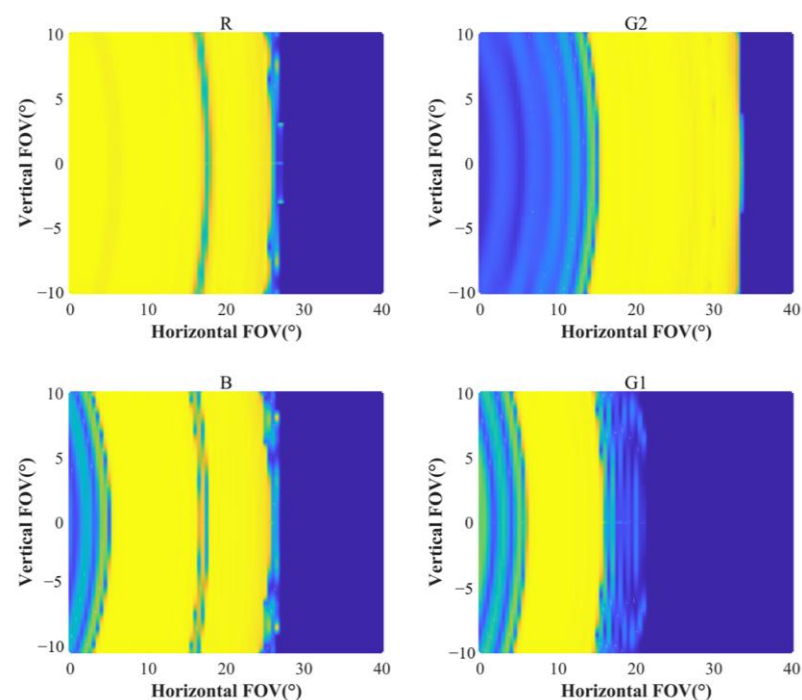


**Figure 6.** Efficiency distribution of horizontal FOV and vertical FOV in the R+G2 waveguide and B+G1 waveguide. The input wavelengths are 633 nm for red, 519 nm for blue and 448 nm for blue.

### 3. Device Fabrication and Results

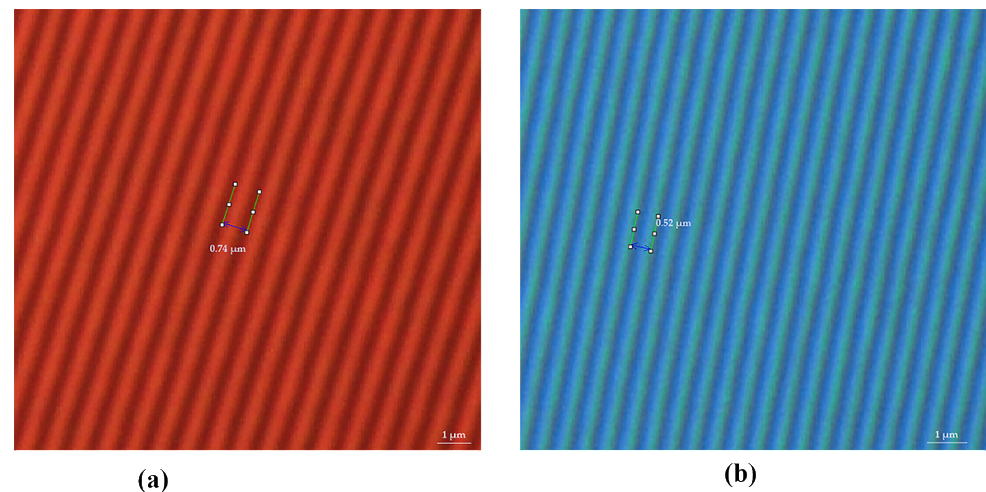
The experimental procedure was similar to that described in [20] except for the different chiral agent concentrations (mass ratio of chiral agent to photocurable monomer) and exposure angles. The azo-dye brilliant yellow (0.5 wt.% BY in DMF) is coated onto the cleaned glass substrate to form a photo-alignment (PA) layer. A substrate with a PA layer is exposed with a 457 nm laser using a polarization interference, after which a solution with a chiral agent liquid crystal mixture is then coated onto the PA layer. For each layer of PVG, the preparation parameters are shown in Table 2. Since there are several solutions

with different chiral agent concentrations, we first coat one of these solutions and cure it. The PVG film formed after curing can be used as a new PA layer. As there are a variety of solutions with different chiral agent concentrations, the previous layer of PVG with a certain concentration is cured, and then another concentration of solutions is coated in the same way.

**Table 2.** Preparation parameters of different PVGs.

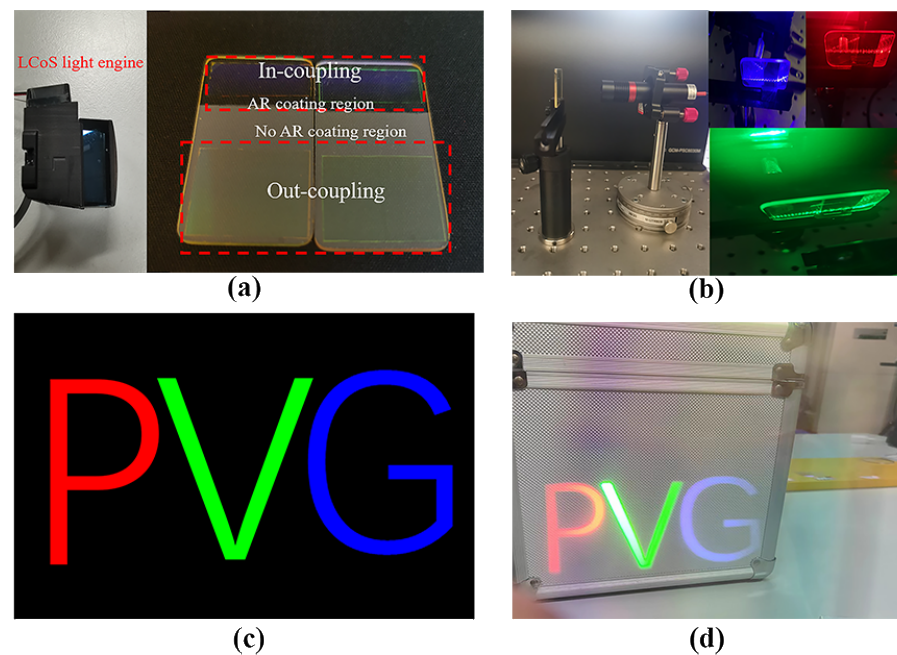
	Exposure Angle (°)	Chiral Agent Concentration
R+G2 waveguide	18	0.018042
	18	0.014855
	18	0.020443
B+G1 waveguide	26	0.025618
	26	0.021201

Figure 7a,b present the polarized optical microscope (POM, Nikon, LV100N) images of R+G2 PVG and B+G1 PVG. We have marked the lateral period of the PVG in the POM images. The measured lateral period of R+G2 PVG is  $0.74\ \mu\text{m}$ , and that of B+G1 PVG is  $0.52\ \mu\text{m}$ , which is basically consistent with the design value.



**Figure 7.** The POM images of PVGs. (a) R+G2. (b) B+G1.

As mentioned before, to prevent crosstalk, we set the two waveguides to have different polarization responses. Also, to prevent reflection loss from the glass surface due to tilted incidence, we coated the glass substrate with the anti-reflection (AR) film in the in-coupling grating region. The prepared waveguide samples are shown in Figure 8a (Right). The refractive index of the substrate used here was 1.57, and each waveguide contained in-coupling gratings and out-coupling gratings. We can see from the figure that the transmittance near the in-coupling grating is significantly higher than the rest of the waveguide. We used lasers with wavelengths of 630 nm (red), 532 nm (green) and 457 nm (blue) as incident light tilted at  $27^\circ$  into the in-coupling grating to observe the coupling transmission function of the prepared waveguide, and the photographs taken are shown in Figure 8b. A simple demonstration model was assembled, with the laser built on a rotating table. The three wavelengths of light can propagate within the waveguides, demonstrating the good coupling capability of the waveguides.



**Figure 8.** (a) Waveguide physical diagram. (b) Coupling propagation capability of the prepared PVG waveguides for 457 nm, 532 nm, and 630 nm laser incident beams. (c) Input image. (d) Output image.

To verify the display effect, we used a 45° FOV LCoS light engine (Figure 8a (Left)). The input image of the microdisplay is shown in Figure 8c, and the final imaging effect is shown in Figure 8d. It can be seen that the resulting image contains the color information of red, green and blue, while the black background of the original image becomes transparent in the resulting virtual image so that the human eye can observe the surrounding environment through the waveguide without hindrance.

#### 4. Conclusions

In this paper, we develop methods for determining the FOV of PVG-based color waveguide display systems. The FOV of a PVG-based color waveguide display is analyzed. The maximum FOV that can be supported by the waveguide is related to the PVG refractive index as well as the lateral period and is, in essence, actually influenced by the diffraction angle. Theoretically, when the refractive index of the PVG is about 1.57, the FOV of the dual-layer waveguide structure can be up to about 60°. However, the tilt angle between the waveguide and the light engine will be very large at this time, which is not advocated in practical applications. Therefore, in this paper, a double-layer color structure with an acceptable range of tilt angle is designed, and a waveguide display with a 45° diagonal FOV is simulated and experimentally realized. Future studies should examine issues of color uniformity and brightness performance.

**Author Contributions:** Conceptualization, Y.G.; Data curation, Y.G. and Y.W.; Formal analysis, R.W. and N.L.; Funding acquisition, Y.W., Y.Z. and B.W.; Investigation, W.W. and L.Z.; Methodology, Y.G. and Y.W.; Resources, Y.G.; Supervision, Y.Z. and B.W.; Validation, Y.G., Y.W. and C.W.; Writing—original draft, Y.G.; Writing—review & editing, Y.G., Y.W. and Y.Z. All authors have read and agreed to the published version of the manuscript.

**Funding:** This work was supported by the ‘National Natural Science Foundation of China (No. 6210031456)’, and the ‘Basic Research Program of Jiangsu Province (No. BK20212006)’.

**Data Availability Statement:** The data presented in this study are available on request from the corresponding author.

**Conflicts of Interest:** The authors declare no conflict of interest.

## References

1. Todorov, T.; Nikolova, L.; Tomova, N. Polarization holography. 1: A new high efficiency organic material with reversible photoinduced birefringence. *Appl. Opt.* **1984**, *23*, 4309–4312. [[CrossRef](#)] [[PubMed](#)]
2. Pancharatnam, S. Generalized theory of interference and its applications. *Proc. Indian Acad. Sci. Sect. A* **1956**, *44*, 398–417. [[CrossRef](#)]
3. Yoo, C.; Bang, K.; Chae, M.; Lee, B. Extended-viewing-angle waveguide near-eye display with a polarization-dependent steering combiner. *Opt. Lett.* **2020**, *45*, 2870–2873. [[CrossRef](#)] [[PubMed](#)]
4. Kim, J.; Li, Y.; Miskiewicz, M.N.; Oh, C.; Kudenov, M.W.; Escuti, M.J. Fabrication of ideal geometric-phase holograms with arbitrary wavefronts. *Optica* **2015**, *2*, 958–964. [[CrossRef](#)]
5. Gao, K.; Cheng, H.H.; Bhowmik, A.K.; Bos, P.J. Thin-film Pancharatnam lens with low f-number and high quality. *Opt. Express* **2015**, *23*, 26086–26094. [[CrossRef](#)]
6. He, Z.; Lee, Y.; Chen, R.; Chanda, D.; Wu, S. Switchable Pancharatnam–Berry microlens array with nano-imprinted liquid crystal alignment. *Opt. Lett.* **2018**, *43*, 5062–5065. [[CrossRef](#)]
7. Zhan, T.; Lee, Y.H.; Wu, S.T. High-resolution additive light field near-eye display by switchable Pancharatnam–Berry phase lenses. *Opt. Express* **2018**, *26*, 4863–4872. [[CrossRef](#)]
8. Chen, Q.; Peng, Z.; Li, Y.; Liu, S.; Zhou, P.; Gu, J.; Lu, J.; Yao, L.; Wang, M.; Su, Y. Multi-plane augmented reality display based on cholesteric liquid crystal reflective films. *Opt. Express* **2019**, *27*, 12039–12047. [[CrossRef](#)]
9. Weng, Y.; Xu, D.; Zhang, Y.; Li, X.; Wu, S. Polarization volume grating with high efficiency and large diffraction angle. *Opt. Express* **2016**, *24*, 17746–17759. [[CrossRef](#)]
10. Kobashi, J.; Yoshida, H.; Ozaki, M. Planar optics with patterned chiral liquid crystals. *Nat. Photonics* **2016**, *10*, 389–392. [[CrossRef](#)]
11. Xiang, X.; Kim, J.; Escuti, M.J. Bragg polarization gratings for wide angular bandwidth and high efficiency at steep deflection angles. *Sci. Rep.* **2018**, *8*, 7202. [[CrossRef](#)] [[PubMed](#)]
12. Xiang, X.; Kim, J.; Komanduri, R.; Escuti, M.J. Nanoscale liquid crystal polymer Bragg polarization gratings. *Opt. Express* **2017**, *25*, 19298–19308. [[CrossRef](#)] [[PubMed](#)]
13. Gao, K.; McGinty, C.; Payson, H.; Berry, S.; Vornehm, J.E.; Finnemeyer, V.A.; Roberts, B.; Bos, P.J. High-efficiency large-angle Pancharatnam phase deflector based on dual-twist design. *Opt. Express* **2017**, *25*, 6283–6293. [[CrossRef](#)]
14. Lee, Y.; Yin, K.; Wu, S. Reflective polarization volume gratings for high efficiency waveguide-coupling augmented reality displays. *Opt. Express* **2017**, *25*, 27008–27014. [[CrossRef](#)] [[PubMed](#)]
15. Li, Y.; Zhan, T.; Wu, S. Flat cholesteric liquid crystal polymeric lens with low f-number. *Opt. Express* **2020**, *28*, 5875–5882. [[CrossRef](#)]
16. Yin, K.; He, Z.; Wu, S. Reflective Polarization Volume Lens with Small f-Number and Large Diffraction Angle. *Adv. Optical Mater.* **2020**, *8*, 2000170. [[CrossRef](#)]
17. Xiong, J.; Li, Y.; Li, K.; Wu, S. Aberration-free pupil steerable Maxwellian display for augmented reality with cholesteric liquid crystal holographic lenses. *Opt. Lett.* **2021**, *46*, 1760–1763. [[CrossRef](#)]
18. Weng, Y.; Zhang, Y.; Cui, J.; Liu, A.; Shen, Z.; Li, X.; Wang, B. Liquid-crystal-based polarization volume grating applied for full-color waveguide displays. *Opt. Lett.* **2018**, *43*, 5773–5776. [[CrossRef](#)]
19. Zhang, Y.; Cui, J. Exit pupil expansion based on polarization volume grating. *Crystals* **2021**, *11*, 333.
20. Gu, Y.; Weng, Y.; Wei, R.; Shen, Z.; Wang, C.; Zhang, L.; Zhang, Y. Holographic waveguide display with large field of view and high light efficiency based on polarized volume holographic Grating. *IEEE Photonics J.* **2022**, *14*, 1–7. [[CrossRef](#)]
21. Xiong, J.; Chen, R.; Wu, S. Device simulation of liquid crystal polarization gratings. *Opt. Express* **2019**, *27*, 18102–18112. [[CrossRef](#)] [[PubMed](#)]
22. Xiong, J.; Yin, K.; Li, K.; Wu, S. Holographic Optical Elements for Augmented Reality: Principles, Present Status, and Future Perspectives. *Adv. Photonics Res.* **2021**, *2*, 2000049. [[CrossRef](#)]